9. V. M. Kapinos, V. Ya. Levchenko, A. F. Slitenko, et al., "Experimental study of the effect of the thermal factor and turbulence of a running flow at the change-over into a boundary layer," Inzh. Fiz. Zh., 32, No. 3 (1977).

# STRUCTURE OF A RISING THERMAL

S. Yu. Gorbunov, B. N. Gordeichik, A. P. Darintsev, V. N. Zabavin, B. V. Zamyshlyaev, B. I. Zaslavskii, A. T. Onufriev, and M. D. Shcherbin

UDC 532.517.4

In [1], the motion was considered for a mass of air heated to a high temperature and initially at rest in a spherical volume under gravity. At the start of the motion, the volume is transformed to a buoyant vortex ring. The turbulent transport in the vortex ring motion is described by a semiempirical theory, which incorporates the effects from the velocity and temperature inhomogeneity, which tend to suppress radial turbulent diffusion fluxes at the core. Numerical calculations have given the distributions for the velocity, vorticity, temperature, and heat fluxes. The toroidal vortex is clearly seen, whose disposition in space coincides with the toroidal temperature pattern.

At an early stage, the main part is played by inertial dynamic effects associated with the generation of the vorticity, which transforms the spherical volume of light gas into a rising vortex ring. The effects from turbulent exchange in the initial stage are neglected because they are slight. The ring formation is described by gas-dynamic equations, which are solved numerically via the [2-4] scheme, which has low scheme viscosity. The gas-dynamic parameter patterns calculated for the formation of the toroidal vortex act as initial ones for calculating the flow structure in the next stage.

Our numerous calculations on structures in thermals have shown that the vortex flow has a decisive effect on the dynamics. One has anisotropy in the turbulent transport, with the turbulent fluxes of heat and momentum diminishing toward the ring axis, which means that the form of the thermal persists for a long time during the rise, while the cross-sectional area of the core increases somewhat, as is observed in [5].

Later calculations were performed on these rings without allowance for the turbulent exchange at the stage of developed vortex motion, which showed that there are only minor differences in the height to which they rise. This shows that there is a decisive influence from inertial dynamic effects associated with the generation of the vorticity field under gravity as regards the rise of a large-scale thermal formation in the atmosphere.

1. This method is applied to experiments on thermals rising in the atmosphere [6] and under laboratory conditions [7]. The velocity and temperature patterns have been calculated without allowance for the turbulent transport. Those patterns have then been used to determine the turbulent characteristics on the assumption of local balance in the turbulent motion. One can judge the justification for this approximation from a comparison with experiment.

We used an r, z, $\varphi$ cylindrical coordinate system. The z axis is directed in the opposite sense to the gravitational acceleration. All the functions are dependent only on r and z. The gas-dynamic equations are

$$\frac{\partial}{\partial t}\rho + \operatorname{div}(\rho\mathbf{V}) = 0,\ \frac{\partial}{\partial t}\mathbf{V} + (\mathbf{V}\cdot\nabla)\mathbf{V} = -\frac{1}{\rho}\nabla p + \mathbf{g},$$
$$\frac{\partial}{\partial t}\left(\rho\varepsilon + \rho\frac{V^2}{2}\right) + \operatorname{div}\left[\mathbf{V}\left(p + \rho\varepsilon + \rho\frac{V^2}{2}\right)\right] = 0, \tag{1.1}$$
$$p = (\gamma - 1)\rho\varepsilon,\ \varepsilon = c_V T,\ \mathbf{V} = (U, V).$$

Dolgoprudnyi. Translated from Prikladnaya Mekhanika i Tekhnicheskaya Fizika, No. 5, pp. 70-76, September-October, 1992. Original article submitted August 23, 1991.

 0021-8944/92/3305-0680$12.50 

Here p, ρ, and T are the pressure, density, and temperature, U and V are the velocity components along the r and z axes, $c_V$ the specific heat at constant volume, and γ the adiabatic parameter.

A finite-difference net containing rectangular cells is introduced, whose boundaries are displaced in space on a definite law in such a way that the thermal remains approximately at the center of the working region.

2. A method of deriving the turbulence spectral characteristics is considered. The local-balance hypothesis is applied to the equations for the turbulent energy and the turbulent pulsation intensity, which gives

$$\frac{2}{3}E\operatorname{div}\mathbf{V}-K_n\left\{2\left[\left(\frac{\partial U}{\partial r}\right)^2+\left(\frac{\partial V}{\partial z}\right)^2+\left(\frac{U}{r}\right)^2\right]+\left(\frac{\partial V}{\partial r}+\frac{\partial U}{\partial z}\right)^2-\frac{2}{3}(\operatorname{div}\mathbf{V})^2\right\}+\varepsilon_t=0; \tag{2.1}$$

$$\frac{V^2K_n+U^2K_s}{V_s^2}\left(\frac{\partial T}{\partial r}\right)^2+\frac{U^2K_n+V^2K_s}{V_s^2}\left(\frac{\partial T}{\partial z}\right)^2+2\frac{UV}{V_s^2}(K_s-K_n)\frac{\partial T}{\partial r}\frac{\partial T}{\partial z}+\varepsilon_\theta=0, \tag{2.2}$$

in which E is the kinetic energy in the turbulence, $\varepsilon_t = B_1E^{3/2}/L_n$ the turbulent energy dissipation rate, $\varepsilon_\theta = (c\beta_4/B)(E^{1/2}\langle\theta^2\rangle/L_n)$ the rate at which the pulsating temperature field is smoothed out, $V_s^2 = U^2 + V^2$, $K_s = BL_sE^{1/2}$, and $K_n = BL_nE^{1/2}$ the turbulent viscosity coefficients along the tangent and along the normal to a stream line, $L_s = \beta_3 L$ the turbulence scale along the tangent to a stream line, L the characteristic flow dimension (diameter of the rising thermal), $L_n$ the scale of the turbulence along the normal to a stream line,

$$L_n/L_s=\left[1+\beta_1\frac{\tau^2V_s^2}{R_n}\frac{1}{T}\frac{\partial T}{\partial n}+\beta_2\frac{2\tau^2V_s^2}{R_n}\left(\frac{\partial U}{\partial z}-\frac{\partial V}{\partial r}\right)\right]^{-1}$$

the relation between the turbulence scales, which was introduced in [1] to incorporate the anisotropy in the turbulent transport, $R_n$ the radius of curvature of the stream line, $\tau = AL_sE^{-1/2}$ the time scale of the turbulence, $\langle\theta^2\rangle$ the temperature pulsation intensity, and $\partial/\partial n$ the derivative along the normal to the stream line. Values used for constants: $\beta_1 = 0.1$, $\beta_2 = 0.1$, $\beta_3 = 0.01$, $A = 3.86$, $B = 4/3$, $\beta_4 = 0.7$, $c = 0.325$, $B_1 = 0.26$.

The effects were incorporated from the vorticity at the core of the vortex on the turbulent transport parametrically at each point with the local radius of curvature for the stream line.

The [8-11] algorithm was used to determine the spectral and integral characteristics, where approximations were used for the spectrum in the low wave number range and in the inertial and dissipative subintervals [12, 13], for which we constructed a universal spectral dependence (generalized Karman model), which approximated the spectrum throughout the wave-number range for the scalar field for a homogeneous isotropic distribution* (here the simplest model, $\mathrm{Pr} \leq 1$):

$$\widehat{E}_\theta=A_1\beta_\theta\frac{y}{(y+y_0)^{11/6}}\exp\left[-\frac{3}{2}A_1(y+y_0)^{2/3}\right],\quad y=\widehat{k}^2.$$

The one-dimensional spectrum is derived from

$$\widehat{E}_{1\theta}=\int_{\widehat{k}_1}^{\infty}\frac{\widehat{E}_\theta}{\widehat{k}}d\widehat{k},\quad\frac{1}{\beta_\theta}=6\int_0^{\infty}\widehat{k}^2\frac{\widehat{E}_{1\theta}(\widehat{k})}{\beta_\theta}d\widehat{k}.$$

In this model, the spectra are dependent on S and $\mathrm{Re}_\lambda$:

$$\widetilde{E}=\frac{E}{\nu^{5/4}\varepsilon_t^{1/4}}=F(\widetilde{k},\mathrm{Re}_\lambda),\quad\widetilde{k}=k\eta,$$

$$\widehat{E}_\theta=\frac{E_\theta}{\varepsilon_\theta\varepsilon_t^{-3/4}D^{5/4}}=F_\theta(\widehat{k}_\theta,S),\quad\widehat{k}_\theta=k\eta_\theta.$$

It was assumed that the spectral distributions in the real flow, which are represented in correspondingly normalized form, are close to these universal distributions with the lo-

*P. G. Zaets derived the spectral distribution in the form given here.

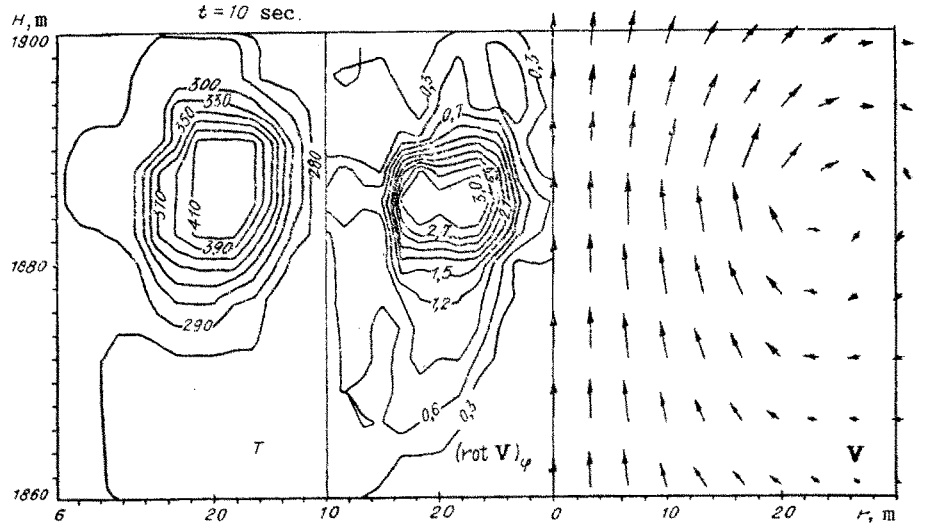


Fig. 1

cally determined $Re_\lambda$ and S. The error is dependent of course on the inhomogeneity and lack of isotropy in the flow. Here $S = Pe_{\lambda\theta}^2/Re_\lambda Pr^{1/2}$ is a parameter enabling one to represent the spectral dependence in universal form, while $Re_\lambda = ((2/3)E)^{1/2}(\lambda/\nu)$, $Pe_{\lambda\theta} = ((2/3)E)^{1/2}\cdot(\lambda_\theta/D)$ are the Reynolds and Peclet numbers corresponding to the Taylor microscales, $Pr = \nu/D$ is the Prandtl number, $\lambda^2 = 10\nu E/\varepsilon_t$, $\lambda_\theta^2 = 12D\langle\theta^2\rangle/\varepsilon_\theta$ are the Taylor microscales for the velocity pulsations (transverse) and temperature, $\eta = (\nu^3/\varepsilon_t)^{1/4}$, $\eta_\theta = (D^3/\varepsilon_t)^{1/4}$ are the Kolmogorov and Corrsin microscales, $\nu$ the kinematic viscosity, and D the thermal diffusivity.

The integral correlation scales are defined from formulas that approximate the calculated curves:

$$\Lambda/\eta = Re_\lambda^{1/2}\left[2{,}47 + 0{,}081\,Re_\lambda^{1/2}\left(Re_\lambda^{1/2} - 1\right)\right],$$

$$\Lambda_\theta/\eta_\theta = 4\pi(3/20)^{1/2}\widehat{E}_{1\theta}(\widehat{k}_1 = 0)/S.$$

The algorithm defines the following: E, $\varepsilon_t$, $\langle\theta^2\rangle$, and $\varepsilon_\theta$ from (2.1) and (2.2) with the (1.1) gas-dynamic parameter patterns; the microscales $\lambda$, $\lambda_\theta$, $\eta$, $\eta_\theta$, the parameters $Re_\lambda$, S, $Re_{\lambda\theta}$, and the integral scales $\Lambda$ and $\Lambda_\theta$; and from the $Re_\lambda$ and S at each point in the flow, estimates for the approximate spectral distributions for the pulsations in the velocity $\tilde{E}$ and temperature $\hat{E}_\theta$.

3. The calculations gave the behavior of the flow parameters for the case examined by experiment in [6]: A mixture of oxygen and methane is pumped into a spherical shell, and detonation gives a high temperature, which causes it to rise. Thermoanemometers 18 m above the center of the balloon recorded the temperature, flow speed, and spectral distribution for the temperature pulsations. Cinematography was used to record the external thermal pattern. We also determined from outside the maximum temperature as a function of time. The following initial conditions were selected from the measurements for calculation: temperature of the thermal $T_0 = 2500$ K, radius $a_0 = 13$ m, and position of the center of the thermal above sea level $H_0 = 1800$ m. The conditions in the surrounding medium corresponded to a standard atmosphere.

The gas-dynamic parameter calculations showed that a rising vortex ring forms from the initially spherical thermal. Initially, a vortex layer is formed near the boundary, and at 4-5 sec after the start of rise, this twists and forms the core of the vortex ring.

Figure 1 shows the calculated patterns for the temperature, vorticity, and velocity at 10 sec after the detonation. Figure 2 shows the flow structure at the core of the vortex at 5 sec: the distributions of T, $(\mathrm{rot}\,\mathbf{V})_\varphi$ and V along a horizontal axis passing through the center of the vortex. There are two peaks in the V distribution, which represent the boundaries of the vortex core, where also the main vorticity and buoyancy are localized. The experiments show that the toroidal form is produced in 4-5 sec after detonation. Figure 3 shows the height to which the center of the thermal has risen $H - H_0$ as a function of time (curve 1 from experiment, curve 2 from theory), while Fig. 4 shows the radius of the ring axis $R_1$ as a function of time (curve 1 from experiment, curve 2 from theory). There is sat-

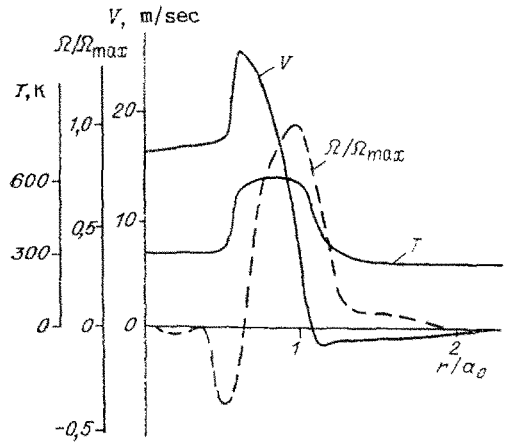


Fig. 2

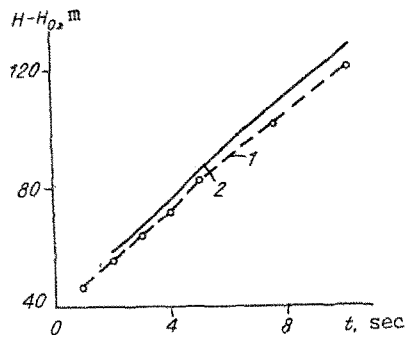


Fig. 3

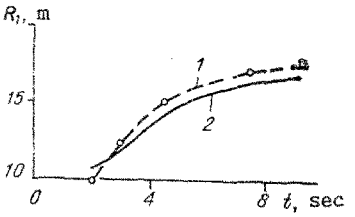


Fig. 4

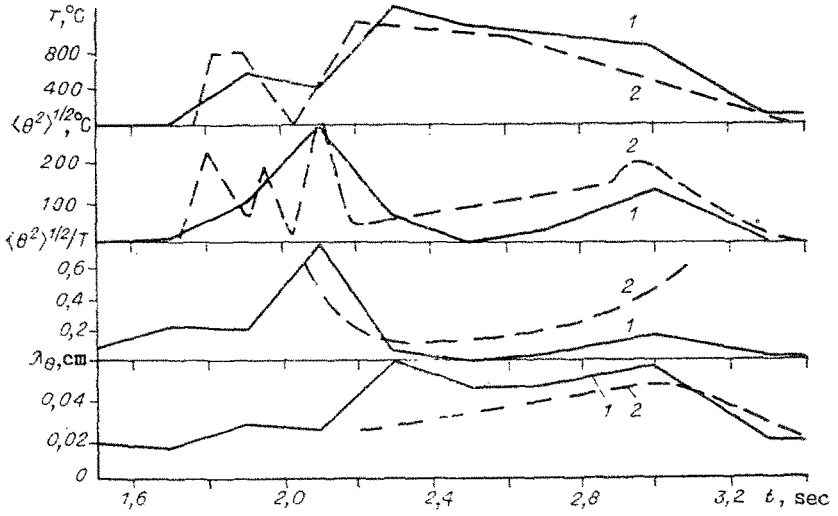


Fig. 5

isfactory agreement between theory and experiment. Figure 5 shows the time course of the averaged gas temperature, the temperature pulsation, and the Taylor microscale for the temperature pulsations (line 1 from theory, line 2 experimental data from [6]). There are three intervals, which correspond to the upper edge of the thermal passing through the sensor system, the central part, and the lower edge. There is good agreement here also.

In [6], values were given for the local Reynolds turbulence number $Re_\lambda = 2000$ and the integral scale $\Lambda_0 = 1$ m. The values obtained in the calculations were $Re_\lambda = 1800$, $\Lambda_\theta = 1.2$ m. The calculated S patterns enable one to estimate some major spectral characteristics in the turbulence.

Figure 6 gives the experimental data for the one-dimensional spectral distributions of the temperature pulsations as a function of the normalized frequency (n frequency, $\tau_1$ sensor signal autocorrelation time) and of the normalized wave number $k\Lambda_\theta$. In the region of large wave numbers, the spectrum is closely approximated by a $-5/3$ law. Curve 1 from [6] is

$$E_{1\theta}(n)/E_{1\theta}(0) = [1 + (2\pi n\tau_1)^2]^{-1} = [1 + (k\Lambda_\theta)^2]^{-1}$$

and approximates the experimental results, with the approximation deteriorating for $k\Lambda_\theta > 100$, while curve 2 is the approximation for the temperature pulsation spectrum constructed via the above algorithm for the estimated S, which is approximately 270. Curve 2 fits the experimental results satisfactorily throughout the wave-number range.

4. One can compare the calculations on thermals in the atmosphere with the [7] experiments from the viewpoint of similarity in structure development for various initial dimensions. In [7], the vortex ring formation was examined for buoyant volumes of a light gas mixture having initial dimensions $a_0 = 0.02$-$0.08$ m and relative density differences $\xi = \Delta\rho/\rho_a = (\rho_a - \rho)/\rho_a = 0.06$-$0.83$ ($\rho_a$ is the gas density in the surrounding medium, while $\rho$ is the density of the gas mixture in the thermal). One uses the variables $z' = z/a_0$, $t' = t/(a_0\rho_a/g\Delta\rho)^{1/2}$ to compare the calculations on the structure with the [7] measurements on the

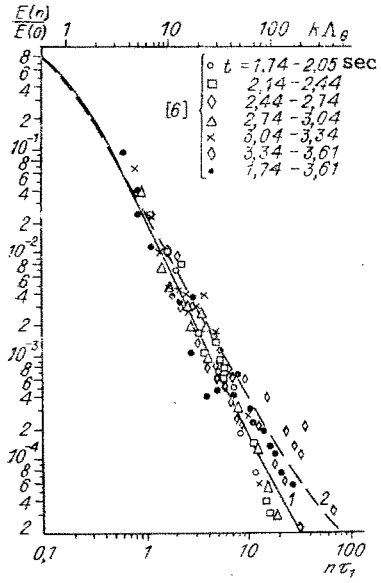


Fig. 6

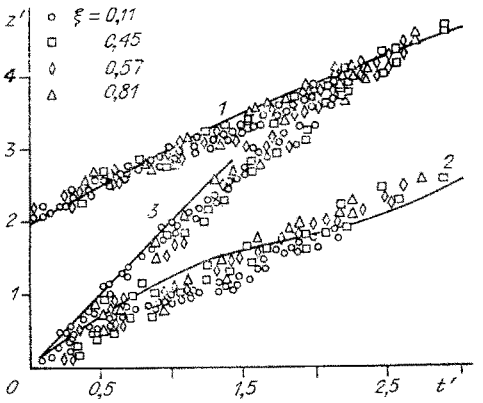


Fig. 7

transformation of a spherical volume of light gas into a toroid. The symbols in Fig. 7 denote the data from laboratory experiments [7] on the time positions of the top edge 1 and lower edge 2 of the model and the upper edge 3 of the jet from the surrounding air layers entering from below along the vertical into the thermal, which transforms the thermal into a toroidal buoyant vortex ring. These data have been obtained by visualizing the flow pattern with an optical knife-edge. Here we give the corresponding curves derived in calculations with the markers initially placed in the surface layers of the spherical thermal. The similarity expresses the fact that one always gets the same process generating the vorticity pattern.

We now consider the applicability of the [1, 7, 10] method as improved here for determining the structure and seek to judge the adequacy of the physical principles used there as regards actual physical processes. The main established fact is that vorticity pattern generation processes predominate in the formation and evolution of thermals in a gravitational field.

Khristianovich in 1954 devised a general scheme for the flow in a large-scale thermal, together with the main element: representation of a thermal as a buoyant vortex ring [14]. We are indebted to S. A. Khristianovich for constant interest in the work and fruitful discussions.

## LITERATURE CITED

1. A. P. Darintsev, V. N. Zabavin, B. V. Zamyshlyaev, et al., "Motion in the atmosphere for a heated mass of air initially in a spherical volume," in: Current Topics in the Mechanics of Continuous Media [in Russian], MFTI, Moscow (1985).
2. D. L. Book and J. P. Boris, "Flux-corrected transport. I. SHASTA. A fluid transport algorithm that works," J. Comput. Phys., 11, No. 1 (1973).
3. D. L. Book, J. P. Boris, and K. Hain, "Flux-corrected transport. II. Generalizations of the method," J. Comput. Phys., 18, No. 3 (1975).
4. V. I. Polezhaev, "Numerical solution to a system of one-dimensional nonstationary Navier–Stokes equations for a compressible gas," Izv. Akad. Nauk SSSR, MZhG, No. 6 (1966).
5. T. Maxworthy, "Turbulent vortex rings," J. Fluid Mech., 64, No. 2 (1974).
6. R. G. Batt, R. A. Bigoni, and D. J. Rowland, "Temperature-field structure within atmospheric buoyant thermals," J. Fluid Mech., 141, 1-25 (1984).
7. B. I. Zaslavskii, "Formation and motion of buoyant vortex rings in homogeneous and stratified media," in: Current Topics in the Mechanics of Continuous Media [in Russian], MFTI, Moscow (1985).
8. R. G. Driscoll and L. A. Kennedy, "A model for the turbulent energy spectrum," Phys. Fluids, 26, No. 5 (1983).
9. P. G. Zaets, A. T. Onufriev, N. A. Safarov, and R. A. Safarov, "Experimental study of the turbulent one-dimensional spectrum function in rotating pipe flow. Importance of the isotropic uniform turbulence model," 5th EPS Liquid State Conf., Moscow, Oct. 1989, Proc., Moscow (1989).

10. P. G. Zaets, A. T. Onufriev, N. A. Safarov, and R. A. Safarov, "An experimental study on the behavior of the energy spectrum in a turbulent flow rotating relative to the longitudinal axis of a tube. Significance of a model for homogeneous isotropic turbulence," Prikl. Mekh. Tekh. Fiz., No. 1 (1992).
11. R. J. Driscoll and L. A. Kennedy, "A model for the spectrum of passive scalars in an isotropic turbulence field," Phys. Fluids, 28, No. 1 (1985).
12. I. O. Hintze, Turbulence [Russian translation], GIFML, Moscow (1963).
13. Y. H. Pao, "Structure of turbulent velocity and scalar fields at large wave numbers," Phys. Fluids, 8, No. 6 (1965).
14. A. T. Onufriev, "Theory of vortex ring motion under gravity: Rise of the cloud from an atomic explosion," Prikl. Mekh. Tekh. Fiz., No. 2 (1967).

# VARIATIONAL PRINCIPLES FOR TWO-PHASE INFILTRATION INTO A DEFORMABLE MEDIUM

P. A. Mazurov

UDC 532.546

Here a method is proposed of constructing dual variational principles for two-phase infiltration into a deformable medium. The construction is based on variational treatments compiled for dissipative and elastic potentials, whose solutions are equivalent to the laws of behavior for the solid and liquid phases. The variational principles enable one to use the known porosity and saturation to determine the displacement and stress patterns in the solid phase and the pressure and velocity patterns in the liquid ones. In the case of two phases, we have variational principles for consolidation theory and two-phase infiltration.

1. Consider two-phase infiltration into a viscoplastic medium. We write [1] the equation of continuity for the solid phase

$$(1-m)_{,t} + \operatorname{div}((1-m)\dot{\mathbf{u}}) = 0; \tag{1.1}$$

the equations of continuity for the liquid phase

$$(ms)_{,t} + \operatorname{div}(ms\mathbf{v}_1) = 0; \tag{1.2}$$

$$(m(1-s))_{,t} + \operatorname{div}(m(1-s)\mathbf{v}_2) = 0; \tag{1.3}$$

the equilibrium equation

$$\sigma^f_{ij,j} - p_{,i} = 0; \tag{1.4}$$

the relation between the pressures in the liquid phases

$$p_1 - p_2 = p_c \tag{1.5}$$

and the entropy production in the energy representation for $T_1 \approx T_2 \approx T_3 \approx \text{const}$ [1]:

$$\Sigma = \sigma^f_{ij}\dot{e}^p_{ij} - \mathbf{q}_1\cdot\nabla p_1 - \mathbf{q}_2\cdot\nabla p_2.$$

Here $\mathbf{u}$ is the vector for the solid-phase displacement; $\mathbf{v}_1$ and $\mathbf{v}_2$ the velocities of the liquid phases; m porosity; s saturation in the first phase; $\sigma_{ij}{}^f$ the components of the tensor for the effective stresses $\boldsymbol{\sigma}^f$; $p = sp_1 + (1-s)p_2$ the mean pressure; $p_1$ and $p_2$ the pressures in the liquid phases; $p_c = p_c(s)$ the capillary pressure step; $e_{ij}{}^p = (1/2)(\dot{u}_{i,j} + \dot{u}_{j,i})$ the components of the tensor for the rates of the viscoplastic strain $\mathbf{e}^p$; $\mathbf{q}_1 = ms(\mathbf{v}_1 - \dot{\mathbf{u}})$, $\mathbf{q}_2 = m(1-s)(\mathbf{v}_2 - \dot{\mathbf{u}})$ the phase infiltration rates; and $T_1$, $T_2$, $T_3$ the absolute temperatures in the phases.

We introduce the symbols $\mathbf{X}_1 = -\nabla p_1$, $\mathbf{X}_2 = -\nabla p_2$, $\mathbf{X}_3 = \boldsymbol{\sigma}^f$, $\mathbf{Y}_1 = \mathbf{q}_1$, $\mathbf{Y}_2 = \mathbf{q}_2$, $\mathbf{Y}_3 = \mathbf{e}^p$ ($\mathbf{X} = (\mathbf{X}_1, \mathbf{X}_2, \mathbf{X}_3)$ for the generalized forces and $\mathbf{Y} = (\mathbf{Y}_1, \mathbf{Y}_2, \mathbf{Y}_3)$ for the generalized velocities. To close system (1.1)-(1.5) we use the normal dissipation hypothesis [2, 3], on which there is a dissipation potential $\varphi(\mathbf{Y})$ and a convex semicontinuous eigenfunctional from below such that

Kazan'. Translated from Prikladnaya Mekhanika i Tekhnicheskaya Fizika, No. 5, pp. 76-82, September-October, 1992. Original article submitted April 4, 1991.